

## Spin-orbit-coupling effects on the valence-band structure of strained semiconductor quantum wells

Calvin Yi-Ping Chao and Shun Lien Chuang

*Department of Electrical and Computer Engineering, University of Illinois, 1406 West Green Street, Urbana, Illinois 61801*

(Received 18 October 1991)

A unitary transformation is found to diagonalize the  $6 \times 6$  Luttinger-Kohn Hamiltonian into two  $3 \times 3$  blocks, making it more efficient to calculate the quantum-well subband structure. Using this formulation, we study systematically the strain-dependent coupling between the heavy-hole bands, light-hole bands, and the spin-orbit split-off bands for a strained quantum well and its bulk limit. We show how the strain deforms the constant energy surface in  $k$  space and compare the subband structure calculated with and without the split-off bands. Our results clearly demonstrate that the spin-orbit coupling has significant effects on the band structure especially for highly strained quantum wells and, therefore, cannot be ignored.

### I. INTRODUCTION

The epitaxial growth of semiconductor layers, which is the key to a variety of important electronic and optoelectronic devices, had long been limited to lattice-matched materials, because the strain and dislocations associated with lattice mismatch are detrimental to device performance. Recently, scientists and engineers began to realize that strain could be a powerful tool for modifying the band structure of semiconductors in a beneficial and predictable way. Since its introduction,<sup>1-3</sup> this concept of strained-layer epitaxy has opened an entirely new dimension in band-gap engineering and device design. Now its application can be found in many major categories of semiconductor devices.

For example, using a strained-layer active region, semiconductor lasers, modulators, or photodetectors can be tuned to a desired operation wavelength with great flexibility. For quantum-well lasers, the splitting of the valence-band edge at  $k = 0$  and the lowering of the in-plane effective mass caused by strain could lead to a decrease of the density of states and the reduction of threshold current.<sup>4,5</sup> The application of a strained-layer heterojunction to the modulation-doped field-effect transistors (MODFET), for instance, using  $\text{In}_{1-x}\text{Ga}_x\text{As}$  rather than GaAs as the conduction channel, has resulted in significantly improved transistor performance,<sup>6-8</sup> primarily due to a larger band offset and better carrier confinement. The use of a strained, graded-band-gap base in a heterojunction bipolar transistor (HBT) also has improved the base transport factor and hence the current gain.<sup>9</sup> Recent surveys on the physics and technology of strained-layer superlattices can be found in Ref. 10.

The effect of strain on the band structure of semiconductors is well understood from the early works of Bir and Pikus,<sup>11</sup> among others.<sup>12-19</sup> For an extensive review on strained-layer semiconductor superlattices, please see Ref. 20. The isotropic (hydrostatic) component of the strain shifts the energy gap; the anisotropic (uniaxial or

shear) component of the strain lifts the degeneracy of the valence bands at  $k = 0$ .

Strain introduces additional coupling between the heavy-hole (HH) bands, light-hole (LH) bands, and the spin-orbit split-off (SO) bands.<sup>21</sup> Such coupling is often ignored, for example, in the calculation of quantum-well subband energies,<sup>22-24</sup> exciton absorption,<sup>25-27</sup> and gain spectra.<sup>28,29</sup> This is justifiable for the lattice-matched system such as  $\text{Al}_x\text{Ga}_{1-x}\text{As}/\text{GaAs}$ . But for highly strained quantum wells, the neglect of the coupling between the HH, LH bands and the SO bands could lead to an error of several tens of meV in energies and up to 30% in effective masses.

The purpose of this paper is to illustrate how the strain modifies the valence-band structure of semiconductors, with the emphasis on the coupling between the HH, LH bands and the SO bands. Our formulation is based on the Luttinger-Kohn Hamiltonian<sup>30,31</sup> and the envelope-function approximation. In Sec. II we derive the analytical formulas of the band-edge energies and the effective masses for a strained bulk semiconductor with or without the SO coupling, and illustrate systematically how the strain deforms the constant energy surface in  $k$  space.

In Sec. III, combining the quantum-size effect with the strain effect, we concentrate on the subband structure calculations for strained quantum wells. Under the axial approximation,<sup>32,33</sup> a unitary transformation is found to diagonalize the  $6 \times 6$  Luttinger-Kohn Hamiltonian into two  $3 \times 3$  blocks. With this simplified Hamiltonian, we then calculate the subband structure of an  $\text{In}_{1-x}\text{Ga}_x\text{As}/\text{InP}$  strained-layer quantum well with and without the SO coupling. Finally, conclusions are given in Sec. IV.

### II. STRAINED BULK SEMICONDUCTOR

Based on the theory of Luttinger-Kohn<sup>30,31</sup> and Bir-Pikus,<sup>11</sup> the valence-band structure of a strained bulk semiconductor can be described by the following  $6 \times 6$  Hamiltonian in the envelope-function space:

$$H = - \begin{bmatrix} \mathcal{P} + \mathcal{Q} & -S & \mathcal{R} & 0 & -\frac{1}{\sqrt{2}}S & \sqrt{2}\mathcal{R} \\ -S^\dagger & \mathcal{P} - \mathcal{Q} & 0 & \mathcal{R} & -\sqrt{2}\mathcal{Q} & \sqrt{\frac{3}{2}}S \\ \mathcal{R}^\dagger & 0 & \mathcal{P} - \mathcal{Q} & S & \sqrt{\frac{3}{2}}S^\dagger & \sqrt{2}\mathcal{Q} \\ 0 & \mathcal{R}^\dagger & S^\dagger & \mathcal{P} + \mathcal{Q} & -\sqrt{2}\mathcal{R}^\dagger & -\frac{1}{\sqrt{2}}S^\dagger \\ -\frac{1}{\sqrt{2}}S^\dagger & -\sqrt{2}\mathcal{Q} & \sqrt{\frac{3}{2}}S & -\sqrt{2}\mathcal{R} & \mathcal{P} + \Delta & 0 \\ \sqrt{2}\mathcal{R}^\dagger & \sqrt{\frac{3}{2}}S^\dagger & \sqrt{2}\mathcal{Q} & -\frac{1}{\sqrt{2}}S & 0 & \mathcal{P} + \Delta \end{bmatrix} \begin{array}{l} |\frac{3}{2}, \frac{3}{2}\rangle \\ |\frac{3}{2}, \frac{1}{2}\rangle \\ |\frac{3}{2}, -\frac{1}{2}\rangle \\ |\frac{3}{2}, -\frac{3}{2}\rangle \\ |\frac{1}{2}, \frac{1}{2}\rangle \\ |\frac{1}{2}, -\frac{1}{2}\rangle \end{array}, \quad (1)$$

where

$$\begin{aligned} \mathcal{P} &= P_k + P_\epsilon, \quad \mathcal{Q} = Q_k + Q_\epsilon, \\ \mathcal{R} &= R_k + R_\epsilon, \quad S = S_k + S_\epsilon, \\ P_k &= \left( \frac{\hbar^2}{2m_0} \right) \gamma_1 (k_x^2 + k_y^2 + k_z^2), \\ Q_k &= \left( \frac{\hbar^2}{2m_0} \right) \gamma_2 (k_x^2 + k_y^2 - 2k_z^2), \\ R_k &= \left( \frac{\hbar^2}{2m_0} \right) \sqrt{3} [-\gamma_2 (k_x^2 - k_y^2) + 2i\gamma_3 k_x k_y], \\ S_k &= \left( \frac{\hbar^2}{2m_0} \right) 2\sqrt{3} \gamma_3 (k_x - ik_y) k_z, \\ P_\epsilon &= -a_v (\epsilon_{xx} + \epsilon_{yy} + \epsilon_{zz}), \\ Q_\epsilon &= -\frac{b}{2} (\epsilon_{xx} + \epsilon_{yy} - 2\epsilon_{zz}), \\ R_\epsilon &= \frac{\sqrt{3}}{2} b (\epsilon_{xx} - \epsilon_{yy}) - id\epsilon_{xy}, \\ S_\epsilon &= -d (\epsilon_{zx} - i\epsilon_{yz}), \end{aligned} \quad (2)$$

where the wave vector  $k$  is interpreted as a differential operator  $-i\nabla$ ;  $\epsilon_{ij}$  is the symmetric strain tensor;  $\gamma_1$ ,  $\gamma_2$ , and  $\gamma_3$  are the Luttinger parameters;  $a_v$ ,  $b$ , and  $d$  are the Bir-Pikus deformation potentials;  $\Delta$  is the spin-orbit split-off energy, and the basis function  $|j, m\rangle$  denotes the Bloch wave function at the zone center (see the Appendix). Here the energy zero is taken to be the top of the unstrained valence band.

The central issue of this paper is to illustrate how the strain modifies the valence-band structures, including the band-edge energies and the effective masses, which are among the most important parameters characterizing any semiconductor materials. We focus on the effects of the coupling between the heavy-hole ( $|\frac{3}{2}, \pm\frac{3}{2}\rangle$ ) bands, light-hole ( $|\frac{3}{2}, \pm\frac{1}{2}\rangle$ ) bands, and the split-off bands ( $|\frac{1}{2}, \pm\frac{1}{2}\rangle$ ). This coupling is commonly considered to be unimportant; therefore, it is neglected in many calculations. For most III-V semiconductors, the split-off bands are several hundred meV below the heavy- and light-hole bands. Since the energy range of interest is only several tens of meV, it is usual to assume that the split-off bands can be safely ignored. In other words, the band structure of the heavy- and light-hole bands is approximately described by the  $4 \times 4$  Hamiltonian

$$H = - \begin{bmatrix} \mathcal{P} + \mathcal{Q} & -S & \mathcal{R} & 0 \\ -S^\dagger & \mathcal{P} - \mathcal{Q} & 0 & \mathcal{R} \\ \mathcal{R}^\dagger & 0 & \mathcal{P} - \mathcal{Q} & S \\ 0 & \mathcal{R}^\dagger & S^\dagger & \mathcal{P} + \mathcal{Q} \end{bmatrix} \begin{array}{l} |\frac{3}{2}, \frac{3}{2}\rangle \\ |\frac{3}{2}, \frac{1}{2}\rangle \\ |\frac{3}{2}, -\frac{1}{2}\rangle \\ |\frac{3}{2}, -\frac{3}{2}\rangle \end{array}. \quad (3)$$

A number of previous calculations on the transition energies of strained quantum wells were based on such an approximation.<sup>22-24</sup> In this paper it is shown, analytically and numerically, that the neglect of the split-off bands can lead to significant errors in both the band-edge energies and effective masses for highly strained semiconductor materials. In this section we deal with the bulk semiconductor, and the effect of quantum confinement in a strained-layer quantum well is discussed in the next section.

The Hamiltonian  $H$  in Eq. (1) is written for an arbitrary strain. For simplicity, in this paper we restrict ourselves to the special case of a biaxial strain, namely,

$$\begin{aligned} \epsilon_{xx} &= \epsilon_{yy} \neq \epsilon_{zz}, \\ \epsilon_{xy} &= \epsilon_{yz} = \epsilon_{zx} = 0, \end{aligned} \quad (4)$$

thus

$$R_\epsilon = S_\epsilon = 0,$$

which essentially covers two of the most important strained systems: (i) a strained-layer semiconductor pseudomorphically grown on a (001)-oriented substrate and (ii) a bulk semiconductor under an external uniaxial stress along the  $z$  direction. For the case of the lattice-mismatched strain, we obtain

$$\begin{aligned} \epsilon_{xx} = \epsilon_{yy} &= \frac{a_0 - a}{a}, \\ \epsilon_{zz} &= -\frac{2C_{12}}{C_{11}} \epsilon_{xx}, \end{aligned} \quad (5)$$

where  $a_0$  and  $a$  are the lattice constants of the substrate and the layer material, and  $C_{11}$  and  $C_{12}$  are the stiffness constants. For the case of external uniaxial stress, we have

$$\begin{aligned} \epsilon_{xx} = \epsilon_{yy} &= \frac{C_{11} + C_{12}}{C_{11}^2 + C_{11}C_{12} - C_{12}^2} T, \\ \epsilon_{zz} &= -\frac{C_{11}}{C_{11}^2 + C_{11}C_{12} - C_{12}^2} T, \end{aligned} \quad (6)$$

where  $T$  is the external stress along the  $z$  axis. The results and conclusions presented in this paper can be easily generalized to other crystal orientations or stress directions. Wherever numerical calculations are needed, we exemplify the ideas on one of the most technologically important systems: strained  $\text{In}_{1-x}\text{Ga}_x\text{As}$  on InP. High-quality and highly strained samples of this system have already been grown and widely studied for optoelectronics applications. All of the material parameters<sup>34</sup> used are listed in Table I, where  $m_e^*$  is the electron effective mass and  $m_0$  is the free-electron mass. All of the parameters for  $\text{In}_{1-x}\text{Ga}_x\text{As}$  are taken as the linear interpolation of those of InAs and GaAs, except that for the strained energy gap,<sup>34</sup>  $E_g(\text{In}_{1-x}\text{Ga}_x\text{As}) = 0.324 + 0.7x + 0.4x^2 + (a_c - a_v)(\epsilon_{xx} + \epsilon_{yy} + \epsilon_{zz})$  is used, where  $a_c$  is the hydrostatic deformation potential for the conduction band. For the conduction- and valence-band offsets, we assume  $\Delta E_c = 0.36\Delta E_g$  and  $\Delta E_v = 0.64\Delta E_g$ .<sup>35</sup>

For the Hamiltonian in Eqs. (1) or (3), the valence-band structure of a bulk semiconductor is determined by the algebraic equation

$$\det [H_{ij}(k) - \delta_{ij} E] = 0, \quad (7)$$

where  $k$  is now interpreted as a real vector and the envelope functions are simply taken as plane waves. For the  $4 \times 4$  Hamiltonian, the solutions of Eq. (7) are simply

$$E_{HH}(k) = -P_\epsilon - P_k - \text{sgn}(Q_\epsilon) \sqrt{(Q_\epsilon + Q_k)^2 + |R_k|^2 + |S_k|^2}, \quad (8)$$

$$E_{LH}(k) = -P_\epsilon - P_k + \text{sgn}(Q_\epsilon) \sqrt{(Q_\epsilon + Q_k)^2 + |R_k|^2 + |S_k|^2},$$

for the heavy holes and light holes, respectively. Each of the solutions is doubly degenerate. Note that it is important to include the sign factor  $\text{sgn}(Q_\epsilon)$  in front of the square root, because  $Q_\epsilon$  could be either negative (compressive strain) or positive (tensile strain) while the square root is conventionally taken as positive. For a finite and fixed strain, the small- $k$  expansion of the above dispersion relation can be written as

TABLE I. Material parameters.

Parameters	GaAs	InAs	InP
$a$ (Å)	5.6533	6.0584	5.8688
$E_g$ (eV)	1.424	0.36	1.344
$\gamma_1$	6.85	20.4	4.95
$\gamma_2$	2.1	8.3	1.65
$\gamma_3$	2.9	9.1	2.35
$C_{11}$ ( $10^{11}$ dyn/cm <sup>2</sup> )	11.879	8.329	10.11
$C_{12}$ ( $10^{11}$ dyn/cm <sup>2</sup> )	5.376	4.526	5.61
$a_c - a_v$ (eV)	-9.77	-6.0	-8.6
$b$ (eV)	-1.7	-1.8	-2.0
$m_e^*/m_0$	0.067	0.027	0.077

$$E_{HH}(k) \approx -P_\epsilon - Q_\epsilon - \left( \frac{\hbar^2}{2m_0} \right) [(\gamma_1 + \gamma_2) k_{\parallel}^2 + (\gamma_1 - 2\gamma_2) k_{\perp}^2], \quad (9)$$

$$E_{LH}(k) \approx -P_\epsilon + Q_\epsilon - \left( \frac{\hbar^2}{2m_0} \right) [(\gamma_1 - \gamma_2) k_{\parallel}^2 + (\gamma_1 + 2\gamma_2) k_{\perp}^2],$$

where  $k_{\perp} = k_z$  and  $k_{\parallel} = \sqrt{k_x^2 + k_y^2}$ , from which we immediately obtain the band-edge energies

$$E_{HH}(0) = -P_\epsilon - Q_\epsilon, \quad (10)$$

$$E_{LH}(0) = -P_\epsilon + Q_\epsilon,$$

and the effective masses parallel ( $\parallel$ ) or perpendicular ( $\perp$ ) to the  $xy$  plane

$$\frac{m_{HH,\perp}^*}{m_0} = \frac{1}{\gamma_1 - 2\gamma_2}, \quad \frac{m_{HH,\parallel}^*}{m_0} = \frac{1}{\gamma_1 + \gamma_2}, \quad (11)$$

$$\frac{m_{LH,\perp}^*}{m_0} = \frac{1}{\gamma_1 + 2\gamma_2}, \quad \frac{m_{LH,\parallel}^*}{m_0} = \frac{1}{\gamma_1 - \gamma_2}.$$

These are the well-known results of Hensel and Feher.<sup>13</sup>

If the split-off bands are included as in the  $6 \times 6$  Hamiltonian, the  $E$ - $k$  relation determined by Eq. (7) becomes a sixth-order polynomial of  $E$ , which apparently can be decomposed into two identical cubic polynomials because of the symmetry property of the Hamiltonian. However, an attempt to expand and factor directly the determinantal equation directly is tedious. The details are given in the Appendix and Eq. (7) is finally reduced to

$$\{\mathcal{E}(k)^3 - 3\lambda(k)\mathcal{E}(k) - \mu(k) + \Delta[\mathcal{E}(k)^2 - \lambda(k)]\}^2 = 0, \quad (12)$$

where

$$\mathcal{E}(k) = E + P_k + P_\epsilon, \quad (13)$$

$$\lambda(k) = (Q_\epsilon + Q_k)^2 + |S_k|^2 + |R_k|^2,$$

$$\mu(k) = 2(Q_\epsilon + Q_k)^3 + 3Q|S_k|^2 - 6Q|R_k|^2 + \frac{3\sqrt{3}}{2}(S^2 R^\dagger + S^{\dagger 2} R).$$

The band-edge energies can be readily solved from Eq. (12) by setting  $k = 0$ ,

$$E_{HH}(0) = -P_\epsilon - Q_\epsilon, \quad (14)$$

$$E_{LH}(0) = -P_\epsilon + \frac{1}{2}(Q_\epsilon - \Delta + \sqrt{\Delta^2 + 2\Delta Q_\epsilon + 9Q_\epsilon^2}),$$

$$E_{SO}(0) = -P_\epsilon + \frac{1}{2}(Q_\epsilon - \Delta - \sqrt{\Delta^2 + 2\Delta Q_\epsilon + 9Q_\epsilon^2}).$$

At  $k = 0$ , the Hamiltonian  $H$  is actually simplified to

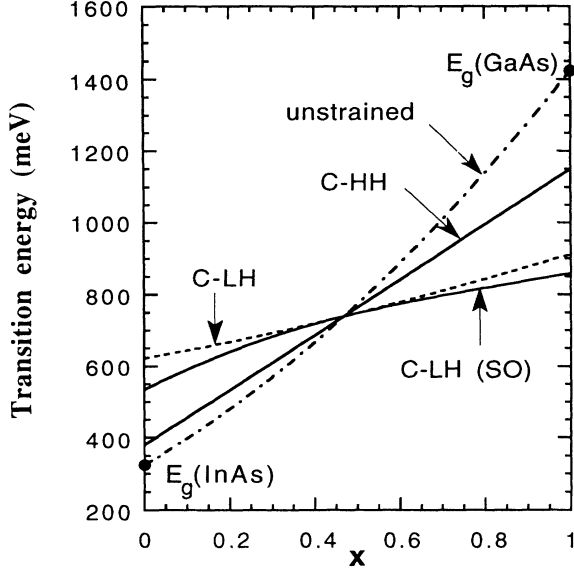


FIG. 1. The energy band gap of a bulk  $\text{In}_{1-x}\text{Ga}_x\text{As}$  vs the Ga mole fraction  $x$ . The dotted-dashed curve: unstrained  $\text{In}_{1-x}\text{Ga}_x\text{As}$ ; the solid curves: transition energies from the conduction band ( $C$ ) to the heavy-hole (HH) and light-hole (LH) bands for a bulk  $\text{In}_{1-x}\text{Ga}_x\text{As}$  pseudomorphically grown on InP; the dashed curve: the conduction to light-hole transition energy calculated without the SO coupling.

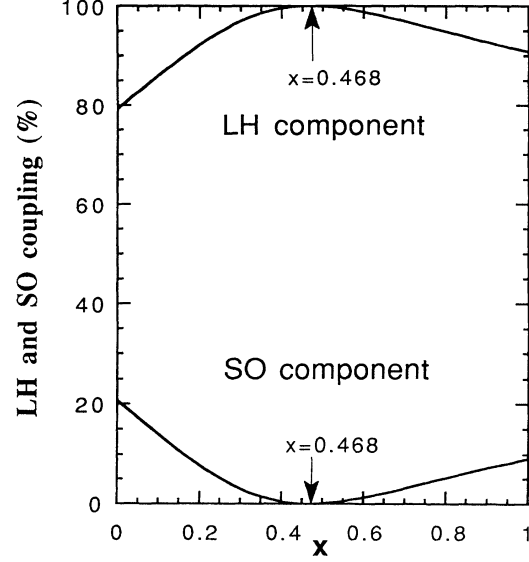


FIG. 2. The percentages of the LH component ( $|F_{3/2,\pm 1/2}|^2$ ) and the SO component ( $|F_{1/2,\pm 1/2}|^2$ ) corresponding to the band-edge energy  $E_{LH}(0)$  [see Eq. (16)] for a bulk  $\text{In}_{1-x}\text{Ga}_x\text{As}$  on InP. This plot shows the strain-dependent coupling between the LH band and the SO band at  $k = 0$ .

$$H(k=0) = - \begin{bmatrix} P_\epsilon + Q_\epsilon & 0 & 0 & 0 & 0 & 0 \\ 0 & P_\epsilon - Q_\epsilon & 0 & 0 & -\sqrt{2}Q_\epsilon & 0 \\ 0 & 0 & P_\epsilon - Q_\epsilon & 0 & 0 & \sqrt{2}Q_\epsilon \\ 0 & 0 & 0 & P_\epsilon + Q_\epsilon & 0 & 0 \\ 0 & -\sqrt{2}Q_\epsilon & 0 & 0 & P_\epsilon + \Delta & 0 \\ 0 & 0 & \sqrt{2}Q_\epsilon & 0 & 0 & P_\epsilon + \Delta \end{bmatrix}. \quad (15)$$

Clearly, the heavy-hole band is decoupled from the rest of bands, while the light-hole band ( $|\frac{3}{2}, \pm\frac{1}{2}\rangle$ ) is coupled with the split-off band ( $|\frac{1}{2}, \pm\frac{1}{2}\rangle$ ) through the strain-dependent off-diagonal terms. This coupling would be totally unaccounted for in the  $4 \times 4$  approximation. For  $\text{In}_{1-x}\text{Ga}_x\text{As}$  on InP, the transition energies from the heavy-hole and the light-hole bands to the conduction band with and without the SO coupling are shown in Fig. 1. The comparison evidently demonstrates how important it is to include the split-off bands, because the error in the light-hole energies could be as large as several tens of meV. The error is comparable to the heavy- and light-hole energy split and is certainly too large to be ignored. As a consequence of the coupling, the eigenvector corresponding to the energy  $E_{LH}(0)$ , determined by

$$\begin{bmatrix} -P_\epsilon + Q_\epsilon & \pm\sqrt{2}Q_\epsilon \\ \pm\sqrt{2}Q_\epsilon & -P_\epsilon - \Delta \end{bmatrix} \begin{bmatrix} F_{3/2,\pm 1/2} \\ F_{1/2,\pm 1/2} \end{bmatrix} = E_{LH}(0) \begin{bmatrix} F_{3/2,\pm 1/2} \\ F_{1/2,\pm 1/2} \end{bmatrix}, \quad (16)$$

$$|F_{3/2,\pm 1/2}|^2 + |F_{1/2,\pm 1/2}|^2 = 1,$$

is not a *pure* light-hole state, but an admixture of the light-hole state and the split-off state. The nature of this

mixing can be quantified and is shown in Fig. 2, the individual light-hole ( $|F_{3/2,\pm 1/2}|^2$ ) and split-off ( $|F_{1/2,\pm 1/2}|^2$ ) components are plotted. For the extreme case of  $x = 0$ , the *light-hole* energy  $E_{LH}(0)$  corresponds to a state with 80% light-hole band characteristics and 20% split-off band characteristics.

The band mixing at finite  $k$  is more complicated since all three bands (HH, LH, and SO) are coupled together. Although it is possible to write down a general, closed-form solution of Eq. (12), physical insights of the strain dependence would be lost in the lengthy expression. In fact, we can calculate the effective masses at  $k = 0$  without solving the cubic equation. First, differentiating Eq. (12) versus  $k_i$  and  $k_j$ , and noting that all the first-order derivatives of  $E(k)$ ,  $\lambda(k)$ , and  $\mu(k)$  vanish at  $k = 0$ , we have

$$\begin{aligned} \left( \frac{\partial^2 E(k)}{\partial k_i \partial k_j} \right)_0 &= \frac{[3\mathcal{E}(0) + \Delta] \left( \frac{\partial^2 \lambda(k)}{\partial k_i \partial k_j} \right)_0 + \left( \frac{\partial^2 \mu(k)}{\partial k_i \partial k_j} \right)_0}{3\mathcal{E}(0)^2 + 2\Delta\mathcal{E}(0) - 3\lambda(0)} \\ &\quad - \left( \frac{\hbar^2}{m_0} \right) \gamma_1 \delta_{ij}. \end{aligned} \quad (17)$$

Substituting in the  $\mathcal{E}(0)$  and evaluating the second-order derivatives of  $\lambda(k)$  and  $\mu(k)$  at  $k = 0$ , we then obtain the series expansion of  $E$  up to the second order of  $k$

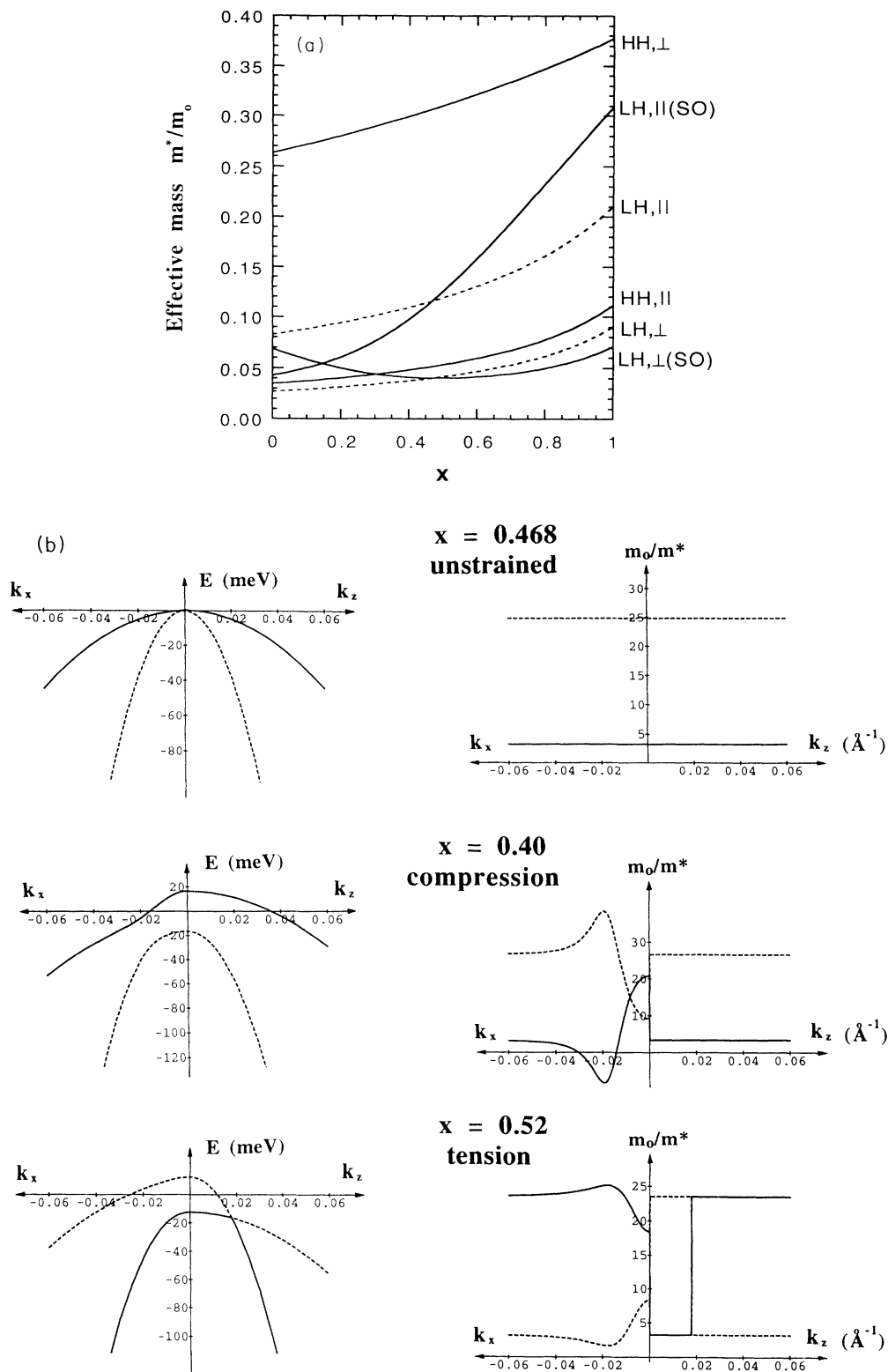


FIG. 3. (a) The heavy-hole (HH) and light-hole (LH) effective masses, at  $k = 0$ , parallel ( $\parallel$ ) and perpendicular ( $\perp$ ) to the growth direction for a bulk  $\text{In}_{1-x}\text{Ga}_x\text{As}$  on InP. The solid curves: with SO coupling; the dashed curves: without SO coupling. (b) The energy  $E$  and the relative reciprocal effective masses  $m_0/m^*$  along the  $k_x$  and  $k_z$  axes; the solid (dashed) curves correspond to heavy (light) holes.

$$E_{HH}(k) \approx E_{HH}(0) - \left( \frac{\hbar^2}{2m_0} \right) [(\gamma_1 + \gamma_2) k_{\parallel}^2 + (\gamma_1 - 2\gamma_2) k_{\perp}^2],$$

$$E_{LH}(k) \approx E_{LH}(0) - \left( \frac{\hbar^2}{2m_0} \right) [(\gamma_1 - f_+ \gamma_2) k_{\parallel}^2 + (\gamma_1 + 2f_+ \gamma_2) k_{\perp}^2], \quad (18)$$

$$E_{SO}(k) \approx E_{SO}(0) - \left( \frac{\hbar^2}{2m_0} \right) [(\gamma_1 - f_- \gamma_2) k_{\parallel}^2 + (\gamma_1 + 2f_- \gamma_2) k_{\perp}^2],$$

where  $f_{\pm}$  is a dimensionless, strain-dependent factor

$$f_{\pm} = \frac{2x [1 + \frac{3}{2} (x - 1 \pm \sqrt{1 + 2x + 9x^2})] + 6x^2}{\frac{3}{4} (x - 1 \pm \sqrt{1 + 2x + 9x^2})^2 + x - 1 \pm \sqrt{1 + 2x + 9x^2} - 3x^2}, \quad x = \frac{Q_{\epsilon}}{\Delta}. \quad (19)$$

From Eq. (18), we obtain the effective masses

$$\frac{m_{HH,\perp}^*}{m_0} = \frac{1}{\gamma_1 - 2\gamma_2}, \quad \frac{m_{HH,\parallel}^*}{m_0} = \frac{1}{\gamma_1 + \gamma_2},$$

$$\frac{m_{LH,\perp}^*}{m_0} = \frac{1}{\gamma_1 + 2f_+ \gamma_2}, \quad \frac{m_{LH,\parallel}^*}{m_0} = \frac{1}{\gamma_1 - f_+ \gamma_2}, \quad (20)$$

$$\frac{m_{SO,\perp}^*}{m_0} = \frac{1}{\gamma_1 + 2f_- \gamma_2}, \quad \frac{m_{SO,\parallel}^*}{m_0} = \frac{1}{\gamma_1 - f_- \gamma_2}.$$

It is interesting to note that  $f_+ = 1$ ,  $f_- = 0$  for the limiting case of zero strain ( $Q_{\epsilon} \rightarrow 0$ ,  $x \rightarrow 0$ ), and the effective masses derived from the  $6 \times 6$  Hamiltonian become identical to those derived from the  $4 \times 4$  Hamiltonian. For the strained-layer  $\text{In}_{1-x}\text{Ga}_x\text{As}$  on  $\text{InP}$ , the effective masses calculated using Eq. (11) (solid curves) and Eq. (20) (dashed curves) are compared in Fig. 3(a). The results for heavy holes are the same whether the SO coupling is included or not, but are quite different for light holes. As shown in Fig. 3(a), the in-plane light-hole effective mass ( $m_{LH,\parallel}^*$ ) would be remarkably underestimated under tension and overestimated under compression if the SO coupling is ignored. The discrepancy could be larger than 30% in the extreme case. However, the notion of the effective mass and the results in Fig. 3(a) should be interpreted with caution. In general, the valence-band energy  $E$  is not exactly a parabolic function of  $k$ ; therefore, the effective mass  $m^*$ , defined by

$$\frac{m_0}{m_{\alpha\beta}^*} = -\frac{m_0}{\hbar^2} \frac{\partial^2 E(k)}{\partial k_{\alpha} \partial k_{\beta}}, \quad \alpha, \beta = x, y, z \quad (21)$$

is not a constant either. Figure 3(a) shows only the effective masses at  $k = 0$ . Solving Eq. (12) numerically, the energy  $E$  and the relative reciprocal effective mass  $m_0/m_{\alpha\beta}^*$  for a bulk  $\text{In}_{1-x}\text{Ga}_x\text{As}/\text{InP}$  as functions of  $k_x$  and  $k_z$  are plotted for (a)  $x = 0.468$  (unstrained), (b)  $x = 0.4$  (compression), and (c)  $x = 0.52$  (tension) in Fig. 3(b).

In Fig. 4 the valence-band structure of  $\text{In}_{1-x}\text{Ga}_x\text{As}/\text{InP}$  is shown schematically. To the left, the energy  $E$  at  $k_y = 0$  is plotted as a function of  $k_x$  and  $k_z$ . To the right,

constant-energy contours are plotted on the  $k_x$ - $k_z$  plane. The label HH or LH is assigned to each band according to its characteristic at the band edge. Comparing these figures, the effects of strain on the valence-band structure can be summarized as follows: (i) the overall energy is shifted by an amount of  $P_{\epsilon}$  due to the valence-band

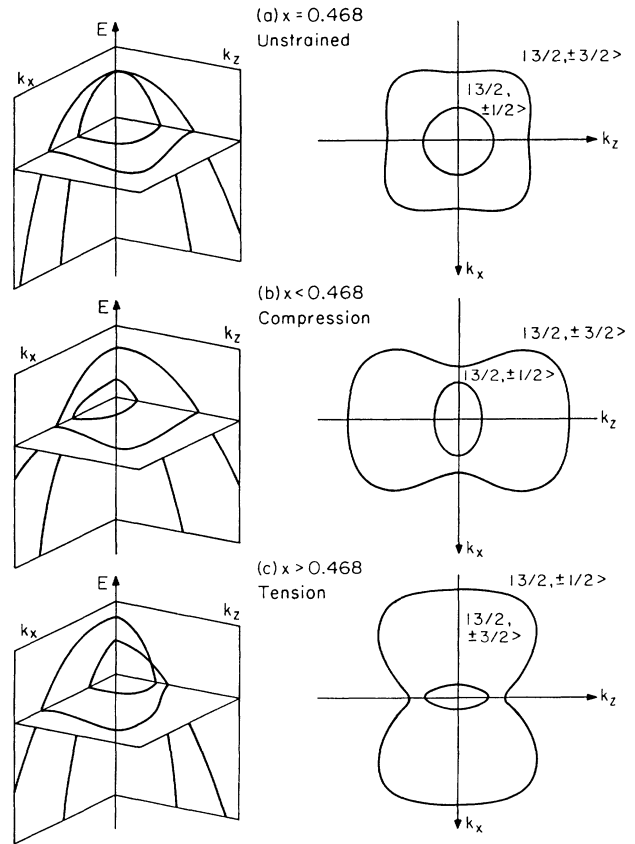


FIG. 4. The valence-band structure of a bulk  $\text{In}_{1-x}\text{Ga}_x\text{As}$  on  $\text{InP}$  substrate for (a)  $x = 0.468$  (lattice-matched), (b)  $x = 0.35$  (compressive strain), and (c)  $x = 0.6$  (tensile strain). On the left: the energy at  $k_y = 0$  as a function of  $k_x$  and  $k_z$ ; on the right: the corresponding constant energy contours in the  $k_x$ - $k_z$  plane.

hydrostatic deformation potential  $a_v$ ; (ii) the originally degenerate valence-band edge at  $k = 0$  is split by an amount  $2Q_\epsilon$  and the HH band can be above or below the LH band depending on whether the strain is tensile or compressive; and (iii) the symmetry of the  $E$ - $k$  relation is reduced from the cubic group  $O$  to the group  $D_{4h}$ .

To visualize the effects of strain systematically, we plot a family of two-dimensional (2D) constant-energy contours at  $k_y = 0$  and the three-dimensional (3D) constant-energy surfaces for the cases of zero strain ( $x = 0.468$ ), compressive strain ( $x = 0.35$ ), and tensile strain ( $x = 0.6$ ) in Figs. 5(a), 5(b), and 5(c), respectively. In each figure, the heavy holes are plotted on the left column and the light holes are plotted on the right column; the 2D contours on the top are plotted for energy  $E$  ranging from the band-edge  $E(0)$  to 30 meV below  $E(0)$ , 3 meV apart between two adjacent curves. Apparently, the shape of the constant-energy surface is independent of  $E$  for the case of zero strain but dependent on  $E$  for the cases of nonzero strain. In Figs. 5(b) and 5(c), the 3D surfaces are plotted for  $E$  equal to 3 meV (in the middle) and 30 meV (on the bottom) below  $E(0)$ , therefore,

corresponding to the innermost and the outermost 2D contours shown in the same figure. At a small energy such as 3 meV below the band edge, the strained  $E$ - $k$  relation in Figs. 5(a) and 5(b) can be well approximated by an ellipsoidal surface with a cylindrical symmetry around the  $z$  direction. As described by the analytical expressions (9) and (18), each semiaxis of the ellipsoid is proportional to the effective mass along the same direction. The heavy hole has a larger effective mass along the  $z$  direction and a smaller effective mass along the  $x$  and  $y$  directions (a prolate ellipsoid), and vice versa for the light hole (an oblate ellipsoid). At 30 meV, the interband coupling is much stronger, the constant-energy surfaces are more deformed, and the parabolic band approximation is no longer valid.

### III. STRAINED-LAYER QUANTUM WELLS

The previous discussion on the valence-band structure of a strained bulk semiconductor is informative, but the numerical results should be interpreted with caution. In practice, a high-quality strained semiconductor layer

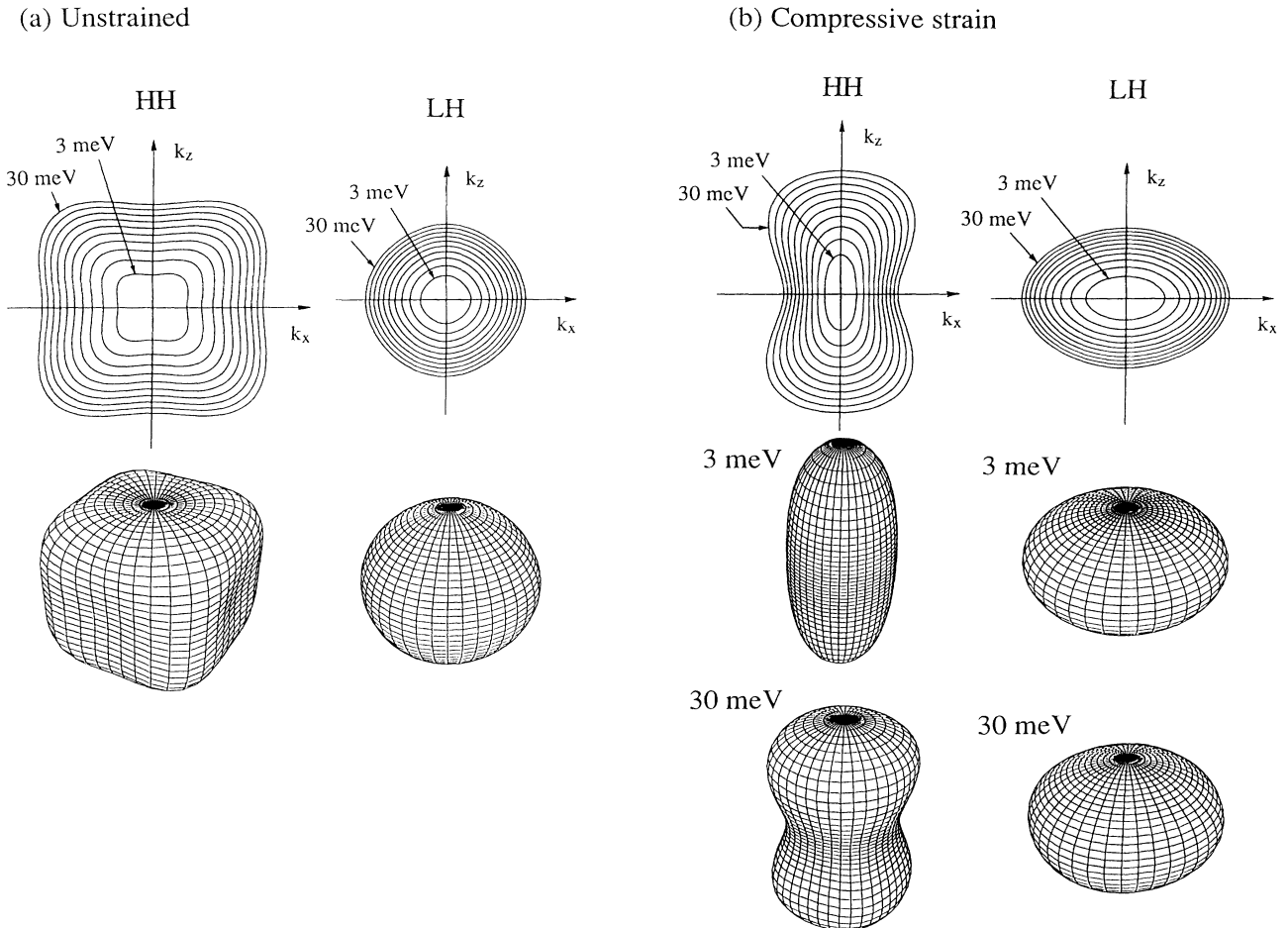


FIG. 5. The 2D constant-energy contours and the 3D constant-energy surfaces of the valence bands for a bulk  $\text{In}_{1-x}\text{Ga}_x\text{As}$  on InP, (a)  $x = 0.468$  (lattice-matched), (b)  $x = 0.35$  (compressive strain), and (c)  $x = 0.6$  (tensile strain). The 2D contours, equally spaced in energy, are plotted from 3 to 30 meV below the band edge. The 3D surfaces in (b) and (c) are plotted for 3 and 30 meV below the band edge.

cannot be grown beyond a certain critical layer thickness (CLT), which strongly depends on the lattice constant mismatch. Therefore, boundary conditions and the quantum-size effects always have to be incorporated. In this section we consider a strained-layer quantum well, assuming that the growth direction is along the  $z$  axis and the strain caused by lattice mismatch is entirely elastically accommodated in the quantum well. The energies and the envelope functions of valence subbands can then be obtained by solving the effective-mass equation

$$\sum_{\nu} [H_{\mu\nu} + V_h(z)\delta_{\mu\nu}] F_{\nu}(\mathbf{k}_{\parallel}, z) = E(\mathbf{k}_{\parallel}) F_{\mu}(\mathbf{k}_{\parallel}, z), \quad (22)$$

$$\mu, \nu \in \left\{ \left| \frac{3}{2}, \frac{3}{2} \right\rangle, \left| \frac{3}{2}, \frac{1}{2} \right\rangle, \left| \frac{3}{2}, -\frac{1}{2} \right\rangle, \left| \frac{3}{2}, -\frac{3}{2} \right\rangle, \left| \frac{1}{2}, \frac{1}{2} \right\rangle, \left| \frac{1}{2}, -\frac{1}{2} \right\rangle \right\},$$

where  $H$  is the Luttinger-Kohn Hamiltonian in Eq. (1) and  $V_h(z)$  is the quantum-well potential for holes. The envelope function component  $F_{\nu}$  has the form

$$F_{\nu}(\mathbf{k}_{\parallel}, \mathbf{r}) = F_{\nu}(\mathbf{k}_{\parallel}, z) e^{i\mathbf{k}_{\parallel} \cdot \boldsymbol{\rho}}, \quad (23)$$

where  $\mathbf{k}_{\parallel} = k_x \hat{\mathbf{x}} + k_y \hat{\mathbf{y}}$ ,  $\boldsymbol{\rho} = x \hat{\mathbf{x}} + y \hat{\mathbf{y}}$ . The Hamiltonian is written in such a way that all of the operators of the form

$$A(z) \frac{\partial^2}{\partial z^2} \text{ and } B(z) \frac{\partial}{\partial z} \quad (24)$$

in Eq. (1) are replaced by

$$\frac{\partial}{\partial z} A(z) \frac{\partial}{\partial z} \text{ and } \frac{1}{2} \left( B(z) \frac{\partial}{\partial z} + \frac{\partial}{\partial z} B(z) \right) \quad (25)$$

to ensure that  $H$  is Hermitian. The proper boundary conditions at the interface between the well and barrier can be obtained by integrating Eq. (22) across the interfaces or by considering the continuity of the probability current density in the envelope-function space.<sup>36</sup> Except for very special cases, such as assuming an infinite barrier height,<sup>37,38</sup> the effective-mass equation does not have analytical solutions; numerical methods must be used. The subband energies and the wave functions, in general, depend not only on the magnitude of the in-plane wave vector  $k_{\parallel}$  but also on the azimuthal angle  $\phi$ , where  $\mathbf{k}_{\parallel} = (k_{\parallel}, \phi)$  in polar coordinates. With this  $\phi$  dependence, the constant-energy contours of the subbands in the  $k_x$ - $k_y$  plane are warped (anisotropic). However, the amount of warping is usually much less than the energy difference between two adjacent subbands. Therefore, it is justifiable to neglect the in-plane anisotropy with-

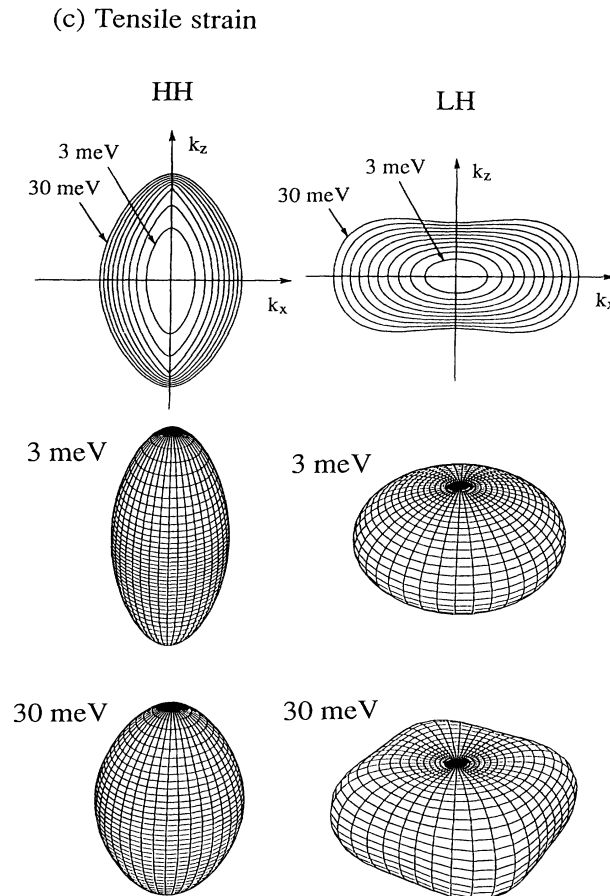


FIG. 5. (Continued).

out losing the essential physics of band mixing. Such an axial (or cylindrical) approximation has been suggested and widely adopted in valence subband calculations using the  $4 \times 4$  Hamiltonian.<sup>32,33</sup> It has been shown that, under the axial approximation, the  $4 \times 4$  Hamiltonian can be block-diagonalized into two  $2 \times 2$  Hamiltonians.<sup>32,33</sup> In this section we extend and apply the axial approximation to the  $6 \times 6$  Hamiltonian and show that it can

be similarly diagonalized into two  $3 \times 3$  blocks. The axial approximation is especially attractive for calculating the binding energies of quantum-well excitons because it simplifies the two-dimensional exciton equation to a one-dimensional equation.<sup>27</sup> Thus, numerical computation becomes much more efficient.

We start with rewriting the matrix elements in Eq. (1) as

$$\begin{aligned} P_k &= \left( \frac{\hbar^2}{2m_0} \right) \gamma_1 (k_{\parallel}^2 + k_z^2), \\ Q_k &= \left( \frac{\hbar^2}{2m_0} \right) \gamma_2 (k_{\parallel}^2 - 2k_z^2), \\ R_k &= - \left( \frac{\hbar^2}{2m_0} \right) \sqrt{3} \left[ \left( \frac{\gamma_2 + \gamma_3}{2} \right) e^{-2i\phi} + \left( \frac{\gamma_2 - \gamma_3}{2} \right) e^{2i\phi} \right] k_{\parallel}^2, \\ S_k &= \left( \frac{\hbar^2}{2m_0} \right) 2\sqrt{3} \gamma_3 k_{\parallel} k_z e^{-i\phi}. \end{aligned} \quad (26)$$

The axial approximation is actually an observation that, if the matrix element  $R_k$  is approximated by

$$R_k \approx - \left( \frac{\hbar^2}{2m_0} \right) \sqrt{3} \left( \frac{\gamma_2 + \gamma_3}{2} \right) k_{\parallel}^2 e^{-2i\phi}, \quad (27)$$

then all of the subband energies will be  $\phi$  independent. To see this, we rotate the reference frame around the  $z$  axis by an angle  $\phi$  and change the basis function  $|j, m\rangle$  into  $|j, m\rangle e^{-im\phi}$  accordingly. The Hamiltonian  $H$  in Eq. (1) becomes

$$H' = - \begin{bmatrix} \mathcal{P} + \mathcal{Q} & -S_{\rho} & R_{\rho} & 0 & -\frac{1}{\sqrt{2}} S_{\rho} & \sqrt{2} R_{\rho} \\ -S_{\rho} & \mathcal{P} - \mathcal{Q} & 0 & R_{\rho} & -\sqrt{2} \mathcal{Q} & \sqrt{\frac{3}{2}} S_{\rho} \\ R_{\rho} & 0 & \mathcal{P} - \mathcal{Q} & S_{\rho} & \sqrt{\frac{3}{2}} S_{\rho} & \sqrt{2} \mathcal{Q} \\ 0 & R_{\rho} & S_{\rho} & \mathcal{P} + \mathcal{Q} & -\sqrt{2} R_{\rho} & -\frac{1}{\sqrt{2}} S_{\rho} \\ -\frac{1}{\sqrt{2}} S_{\rho} & -\sqrt{2} \mathcal{Q} & \sqrt{\frac{3}{2}} S_{\rho} & -\sqrt{2} R_{\rho} & \mathcal{P} + \Delta & 0 \\ \sqrt{2} S_{\rho} & \sqrt{\frac{3}{2}} S_{\rho} & \sqrt{2} \mathcal{Q} & -\frac{1}{\sqrt{2}} S_{\rho} & 0 & \mathcal{P} + \Delta \end{bmatrix} \begin{matrix} |\frac{3}{2}, \frac{3}{2}\rangle e^{-i(3/2)\phi} \\ |\frac{3}{2}, \frac{1}{2}\rangle e^{-i(1/2)\phi} \\ |\frac{3}{2}, -\frac{1}{2}\rangle e^{i(1/2)\phi} \\ |\frac{3}{2}, -\frac{3}{2}\rangle e^{i(3/2)\phi} \\ |\frac{1}{2}, \frac{1}{2}\rangle e^{-i(1/2)\phi} \\ |\frac{1}{2}, -\frac{1}{2}\rangle e^{i(1/2)\phi} \end{matrix}, \quad (28)$$

where

$$\begin{aligned} R_{\rho} &= - \left( \frac{\hbar^2}{2m_0} \right) \sqrt{3} \left( \frac{\gamma_2 + \gamma_3}{2} \right) k_{\parallel}^2, \\ S_{\rho} &= \left( \frac{\hbar^2}{2m_0} \right) 2\sqrt{3} \gamma_3 k_{\parallel} k_z, \end{aligned} \quad (29)$$

and  $R_{\epsilon} = S_{\epsilon} = 0$  by assumption. The new Hamiltonian  $H'$  has the same form as  $H$  with the  $\mathcal{R}$  and  $\mathcal{S}$  replaced by  $R_{\rho}$  and  $S_{\rho}$ , respectively. Note that  $R_{\rho}$  and  $S_{\rho}$  are Hermitian operators while  $\mathcal{R}$  and  $\mathcal{S}$  are not. After rotating the reference frame, we find that each matrix element of  $H'$  is independent of the angle  $\phi$ . As a consequence, the subband energy must also be  $\phi$  independent, that is,  $E(\mathbf{k}_{\parallel}) = E(k_{\parallel})$ . As to the  $\phi$  dependence of the envelope-function components, it is simply  $F_{\nu}(\mathbf{k}_{\parallel}, z) = F_{\nu}(k_{\parallel}, z) e^{-im\phi}$ , where  $\nu = (j, m)$ .<sup>39</sup>

The most important advantage gained from the axial

approximation is that the Hamiltonian  $H'$  can be further block-diagonalized by choosing a new basis set

$$\begin{aligned} |u_1\rangle &= \frac{1}{\sqrt{2}} (|\frac{3}{2}, \frac{3}{2}\rangle e^{-i(3/2)\phi} - i|\frac{3}{2}, -\frac{3}{2}\rangle e^{i(3/2)\phi}), \\ |u_2\rangle &= \frac{1}{\sqrt{2}} (i|\frac{3}{2}, \frac{1}{2}\rangle e^{-i(1/2)\phi} - |\frac{3}{2}, -\frac{1}{2}\rangle e^{i(1/2)\phi}), \\ |u_3\rangle &= \frac{-1}{\sqrt{2}} (i|\frac{1}{2}, \frac{1}{2}\rangle e^{-i(1/2)\phi} + |\frac{1}{2}, -\frac{1}{2}\rangle e^{i(1/2)\phi}), \\ |u_4\rangle &= \frac{1}{\sqrt{2}} (|\frac{3}{2}, \frac{3}{2}\rangle e^{-i(3/2)\phi} + i|\frac{3}{2}, -\frac{3}{2}\rangle e^{i(3/2)\phi}), \\ |u_5\rangle &= \frac{-1}{\sqrt{2}} (i|\frac{3}{2}, \frac{1}{2}\rangle e^{-i(1/2)\phi} + |\frac{3}{2}, -\frac{1}{2}\rangle e^{i(1/2)\phi}), \\ |u_6\rangle &= \frac{1}{\sqrt{2}} (i|\frac{1}{2}, \frac{1}{2}\rangle e^{-i(1/2)\phi} - |\frac{1}{2}, -\frac{1}{2}\rangle e^{i(1/2)\phi}). \end{aligned} \quad (30)$$

Carrying out the associated similarity transformation, we finally obtain a block-diagonalized Hamiltonian

$$H'' = \begin{bmatrix} H_{3 \times 3} & 0 \\ 0 & H_{3 \times 3}^\dagger \end{bmatrix},$$

$$H_{3 \times 3} = - \begin{bmatrix} \mathcal{P} + \mathcal{Q} & -R_\rho - iS_\rho & -\sqrt{2}R_\rho + \frac{i}{\sqrt{2}}S_\rho \\ -R_\rho + iS_\rho & \mathcal{P} - \mathcal{Q} & \sqrt{2}Q + i\sqrt{\frac{3}{2}}S_\rho \\ -\sqrt{2}R_\rho - \frac{i}{\sqrt{2}}S_\rho & \sqrt{2}Q - i\sqrt{\frac{3}{2}}S_\rho & \mathcal{P} + \Delta \end{bmatrix} \begin{matrix} |u_1\rangle \\ |u_2\rangle \\ |u_3\rangle \end{matrix}, \quad (31)$$

and  $H_{3 \times 3}^\dagger$  is the Hermitian conjugate of  $H_{3 \times 3}$ . The original set of six-coupled differential equations (22) is now reduced to two sets of three coupled differential equations, corresponding to the basis sets  $\{u_1, u_2, u_3\}$  and  $\{u_4, u_5, u_6\}$ , respectively. If the potential energy has a reflection symmetry  $V_h(-z) = V_h(z)$ , then only one set of these equations has to be solved, because the other leads to identical subband energies. Since the new basis set only mixes  $|j, m\rangle$  with  $|j, -m\rangle$ , we can still assign the label HH (heavy hole) to the bases  $|u_1\rangle$  and  $|u_4\rangle$ ; LH (light hole) to  $|u_2\rangle$  and  $|u_5\rangle$ ; SO (split-off) to  $|u_3\rangle$  and  $|u_6\rangle$ . When the split-off bands are ignored, we are left with the upper  $2 \times 2$  block of the Hamiltonian  $H_{3 \times 3}$ ,

$$H_{2 \times 2} = - \begin{bmatrix} \mathcal{P} + \mathcal{Q} & -R_\rho - iS_\rho \\ -R_\rho + iS_\rho & \mathcal{P} - \mathcal{Q} \end{bmatrix} \begin{matrix} |u_1\rangle \\ |u_2\rangle \end{matrix}. \quad (32)$$

To study the effect of SO coupling, we now consider a  $\text{In}_{1-x}\text{Ga}_x\text{As}/\text{InP}$  quantum well and compare the subband structures calculated using  $H_{3 \times 3}$  and  $H_{2 \times 2}$ . A numerical method similar to that described in Ref. 24 is used. First, all of the plane-wave solutions in the well and barrier are found and the envelope-function spinor ( $F_\nu, \nu = 1, 2, 3$ ) is written as a linear combination of the plane waves in each region. Then, the subband energies and the coefficients of linear combination are solved by imposing the boundary conditions, that is, requiring the continuity of

$$\begin{bmatrix} F_1(z) \\ F_2(z) \\ F_3(z) \end{bmatrix} \quad (33)$$

and

$$\begin{bmatrix} (\gamma_1 - 2\gamma_2) \frac{\partial}{\partial z} & \sqrt{3}\gamma_3 k_\parallel & -\sqrt{\frac{3}{2}}\gamma_3 k_\parallel \\ -\sqrt{3}\gamma_3 k_\parallel & (\gamma_1 + 2\gamma_2) \frac{\partial}{\partial z} & -\frac{3}{\sqrt{2}}\gamma_3 k_\parallel \\ \sqrt{\frac{3}{2}}\gamma_3 k_\parallel & \frac{3}{\sqrt{2}}\gamma_3 k_\parallel & \gamma_1 \frac{\partial}{\partial z} \end{bmatrix} \begin{bmatrix} F_1(z) \\ F_2(z) \\ F_3(z) \end{bmatrix} \quad (34)$$

across the interfaces between the well and the barriers.

In Fig. 6 the valence subband energies at  $k_\parallel = 0$  for a 60-Å  $\text{In}_{1-x}\text{Ga}_x\text{As}/\text{InP}$  quantum well are plotted versus  $x$ , which shows the dramatic difference between the light-hole energies calculated with (solid curves) and without (dashed curves) the SO coupling. In contrast, the heavy-hole energies (dotted-dashed curves) are not affected by the SO coupling.

The SO coupling not only changes the band-edge energies but also alters the subband structure considerably.

In Figs. 7(a), 7(b), and 7(c), we plot the subband energy  $E$  as a function of  $k_\parallel$  for a 60-Å quantum well with  $x = 0.468$  (no strain),  $x = 0.25$  (compression), and  $x = 0.6$  (tension), respectively. At a finite  $k_\parallel$ , both the LH band and the HH band are modified by the SO coupling. It is also observed that all of the subband energies calculated including the SO coupling (solid curves) are higher than those calculated ignoring the SO coupling (dashed curves). This general trend is not an accident but a direct consequence of the quantum-mechanical level repulsion: the HH and LH bands are pushed upward by the SO band below them.

The effects of strain on the subband structures have been discussed in detail in Ref. 24. For the unstrained quantum well ( $x = 0.468$ ), the first heavy-hole state always lies above the first light-hole state, because the heavy hole has a larger effective mass along the growth direction (quantum-size effect). For the compressively strained quantum well, the heavy-hole state is moved to higher energy and the light-hole state to lower energy due to the shear-deformation potential. The most inter-

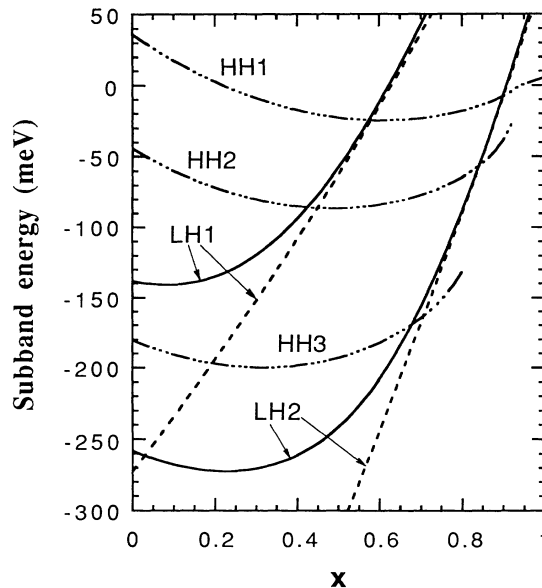


FIG. 6. The valence subband energies at  $k_\parallel = 0$  for a 60-Å  $\text{In}_{1-x}\text{Ga}_x\text{As}$  quantum well sandwiched between InP barriers. The dotted-dashed curves: heavy-hole (HH) subbands; the solid curves: light-hole (LH) subbands including the SO coupling; the dashed curves: light-hole subbands ignoring the SO coupling.

esting case occurs when the strain is tensile; the shear-deformation potential tends to move the light-hole energy upward and heavy-hole energy downward, thus competing with the quantum-size effect. As a result, the subband structure can be engineered such that the highest valence subband can be chosen to be HH or LH band. For the 60-Å well in Fig. 6, the LH1 and HH1 states crossover at  $x \approx 0.58$ . At  $x = 0.6$  shown in Fig. 7(c), the LH1 is above the HH1.

#### IV. CONCLUSIONS

Because of the flexibility of using a variety of materials and the ability to tailor the band offsets, strained-layer semiconductor devices are superior in many ways to the conventional devices based on lattice-matched systems. Understanding and modeling the optoelectronic properties of these devices, such as the gain spectra of quantum-well lasers and the absorption spectra of quantum-well

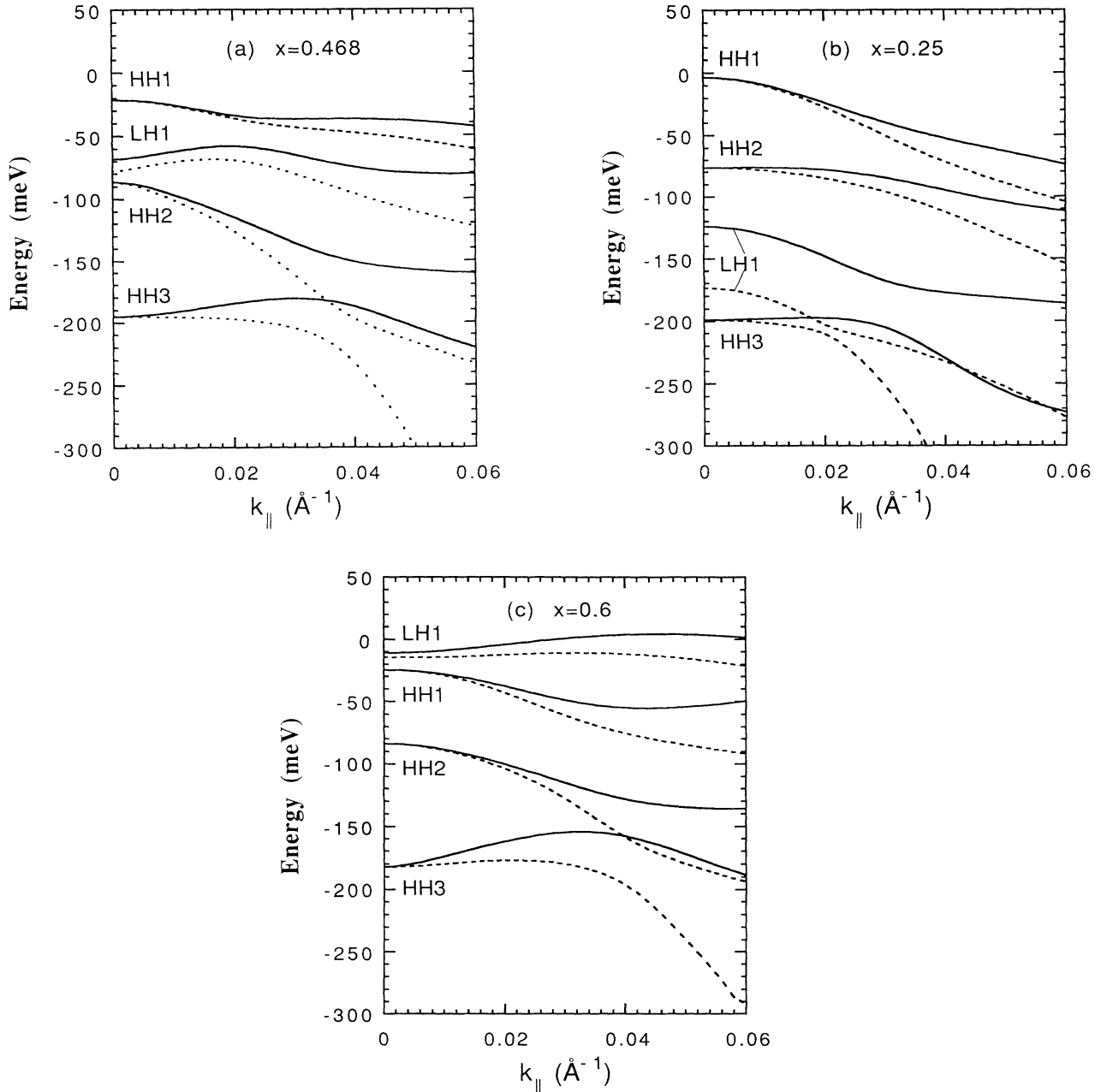


FIG. 7. The valence subband structure for a 60-Å  $\text{In}_{1-x}\text{Ga}_x\text{As}$  quantum well sandwiched between InP barriers for (a)  $x = 0.468$  (lattice-matched), (b)  $x = 0.25$  (compressive strain), and (c)  $x = 0.6$  (tensile strain). The solid curves: including the SO coupling; the dashed curves: ignoring the SO coupling.

modulators, requires knowledge of the accurate subband structure. In this paper we have studied the effects of strain on the valence-band structure. We have shown that the strain would introduce additional coupling between the heavy- and light-hole bands and the spin-orbit split-off bands. We have presented graphically how the strain deformed the constant energy surface in  $k$  space, derived analytical formulas for the hole effective masses, and found a transformation to block-diagonalize the  $6 \times 6$  Luttinger-Kohn Hamiltonian, thus simplifying the subband structure calculation considerably yet retaining the important spin-orbit split-off band coupling. This simplified formulation should be useful for studying the exciton absorption and gain spectrum in highly strained quantum-well devices.

### ACKNOWLEDGMENTS

This work was supported in part by the Office of Naval Research (Grant No. N00014-90-J-1821) and the Joint Services Electronics Program (Grant No. N00014-90-J-1270). The computation time was provided by the National Center for Supercomputer Applications at the University of Illinois, Urbana-Champaign.

### APPENDIX: DISPERSION RELATIONS

The Luttinger-Kohn Hamiltonian in Eq. (1) is written in terms of the basis set

$$\begin{aligned}
 \left| \frac{3}{2}, \frac{3}{2} \right\rangle &= -\frac{1}{\sqrt{2}} |(x + iy) \uparrow\rangle, \\
 \left| \frac{3}{2}, \frac{1}{2} \right\rangle &= \frac{1}{\sqrt{6}} |-(x + iy) \downarrow + 2z \uparrow\rangle, \\
 \left| \frac{3}{2}, -\frac{1}{2} \right\rangle &= \frac{1}{\sqrt{6}} |(x - iy) \uparrow + 2z \downarrow\rangle, \\
 \left| \frac{3}{2}, -\frac{3}{2} \right\rangle &= \frac{1}{\sqrt{2}} |(x - iy) \downarrow\rangle, \\
 \left| \frac{1}{2}, \frac{1}{2} \right\rangle &= \frac{1}{\sqrt{3}} |(x + iy) \downarrow + z \uparrow\rangle, \\
 \left| \frac{1}{2}, -\frac{1}{2} \right\rangle &= \frac{1}{\sqrt{3}} |(x - iy) \uparrow - z \downarrow\rangle.
 \end{aligned} \tag{A1}$$

To factor the associated sixth-order determinant equation (7), we find it convenient to work on a different basis

$$\begin{aligned}
 &\frac{1}{\sqrt{2}} |(x + iy) \uparrow\rangle, \\
 &\frac{1}{\sqrt{2}} |(x - iy) \uparrow\rangle, \\
 &|z \uparrow\rangle, \\
 &\frac{1}{\sqrt{2}} |(x - iy) \downarrow\rangle, \\
 &\frac{1}{\sqrt{2}} |(x + iy) \downarrow\rangle, \\
 &|z \downarrow\rangle.
 \end{aligned} \tag{A2}$$

Because this new basis set transforms  $H$  into a *nearly* block-diagonalized form

$$H' = - \begin{bmatrix} \mathcal{P} + \mathcal{Q} & -\sqrt{3}\mathcal{R} & \sqrt{\frac{3}{2}}\mathcal{S} & 0 & 0 & 0 \\ -\sqrt{3}\mathcal{R}^\dagger & \mathcal{P} + \mathcal{Q} + \frac{2\Delta}{3} & \sqrt{\frac{3}{2}}\mathcal{S}^\dagger & 0 & 0 & -\frac{\sqrt{2}\Delta}{3} \\ \sqrt{\frac{3}{2}}\mathcal{S}^\dagger & \sqrt{\frac{3}{2}}\mathcal{S} & \mathcal{P} - 2\mathcal{Q} + \frac{\Delta}{3} & 0 & \frac{\sqrt{2}\Delta}{3} & 0 \\ 0 & 0 & 0 & \mathcal{P} + \mathcal{Q} & -\sqrt{3}\mathcal{R}^\dagger & \sqrt{\frac{3}{2}}\mathcal{S}^\dagger \\ 0 & 0 & \frac{\sqrt{2}\Delta}{3} & -\sqrt{3}\mathcal{R} & \mathcal{P} + \mathcal{Q} + \frac{2\Delta}{3} & \sqrt{\frac{3}{2}}\mathcal{S} \\ 0 & -\frac{\sqrt{2}\Delta}{3} & 0 & \sqrt{\frac{3}{2}}\mathcal{S} & \sqrt{\frac{3}{2}}\mathcal{S}^\dagger & \mathcal{P} - 2\mathcal{Q} + \frac{\Delta}{3} \end{bmatrix}. \tag{A3}$$

Then, with the help of a mathematical identity,

$$\begin{vmatrix} a_{11} & a_{12} & a_{13} & 0 & 0 & 0 \\ a_{21} & a_{22} & a_{23} & 0 & 0 & x \\ a_{31} & a_{32} & a_{33} & 0 & -x & 0 \\ 0 & 0 & 0 & a_{11} & a_{21} & a_{31} \\ 0 & 0 & -x & a_{12} & a_{22} & a_{32} \\ 0 & x & 0 & a_{13} & a_{23} & a_{33} \end{vmatrix} = \left( \begin{vmatrix} a_{11} & a_{12} & a_{13} \\ a_{21} & a_{22} & a_{23} \\ a_{31} & a_{32} & a_{33} \end{vmatrix} - a_{11}x^2 \right)^2, \tag{A4}$$

and some straightforward algebra, we can immediately simplify Eq. (7) to

$$\det(H'_{ij} - \delta_{ij}E) = \{\mathcal{E}^3 - 3\lambda\mathcal{E} - \mu + \Delta[\mathcal{E}^2 - \lambda]\}^2 = 0, \tag{A5}$$

where

$$\mathcal{E} = E + \mathcal{P}, \quad \lambda = \mathcal{Q}^2 + |\mathcal{S}|^2 + |\mathcal{R}|^2, \quad \mu = 2\mathcal{Q}^3 + 3\mathcal{Q}|\mathcal{S}|^2 - 6\mathcal{Q}|\mathcal{R}|^2 + \frac{3\sqrt{3}}{2}(\mathcal{S}^2\mathcal{R}^\dagger + \mathcal{S}^{\dagger 2}\mathcal{R}). \tag{A6}$$

- <sup>1</sup>G. C. Osbourn, *J. Appl. Phys.* **53**, 1586 (1982).
- <sup>2</sup>G. C. Osbourn, *Phys. Rev. B* **27**, 5126 (1983).
- <sup>3</sup>G. C. Osbourn, *IEEE J. Quantum Electron.* **QE-22**, 1677 (1986).
- <sup>4</sup>E. Yablonovitch and E. O. Kane, *IEEE J. Lightwave Technol.* **LT-4**, 961 (1986).
- <sup>5</sup>A. R. Adams, *Electron. Lett.* **22**, 249 (1986).
- <sup>6</sup>J. J. Rosenberg, M. Benlamri, P. D. Kirchner, J. M. Woodall, and G. D. Pettit, *IEEE Electron. Dev. Lett.* **EDL-6**, 491 (1985).
- <sup>7</sup>P. C. Chao, R. C. Tiberio, K. H. G. Duh, P. M. Smith, J. M. Ballingal, L. F. Lester, B. R. Lee, A. Jabra, and G. G. Gifford, *IEEE Electron. Dev. Lett.* **EDL-8**, 489 (1987).
- <sup>8</sup>L. D. Nguyen, W. J. Schaff, P. J. Tasker, A. N. Lepore, L. F. Palmateer, M. C. Foisy, and L. F. Eastman, *IEEE Trans. Electron. Dev.* **ED-35**, 139 (1989).
- <sup>9</sup>P. M. Enquist, L. P. Ramberg, F. E. Najjar, W. J. Schaff, K. L. Kavanagh, G. W. Wicks, and L. F. Eastman, *J. Cryst. Growth* **81**, 378 (1987).
- <sup>10</sup>*Semiconductors and Semimetals*, edited by R. K. Willardson and A. C. Beer (Academic, New York, 1990), Vols. 32 and 33.
- <sup>11</sup>G. L. Bir and G. E. Pikus, *Symmetry and Strain-Induced Effects in Semiconductors* (Wiley, New York, 1974).
- <sup>12</sup>W. H. Klein and L. M. Roth, *Phys. Rev. Lett.* **2**, 3341 (1959).
- <sup>13</sup>J. C. Hensel and G. Feher, *Phys. Rev.* **129**, 1041 (1963).
- <sup>14</sup>H. Hasegawa, *Phys. Rev.* **129**, 1029 (1963).
- <sup>15</sup>I. Balslev, in *Semiconductors and Semimetals*, edited by R. K. Willardson and A. C. Beer (Academic, New York, 1972), Vol. 9.
- <sup>16</sup>E. O. Kane, *Phys. Rev.* **178**, 1368 (1969).
- <sup>17</sup>F. H. Pollak, *Surf. Sci.* **37**, 863 (1973).
- <sup>18</sup>D. E. Aspnes and M. Cardona, *Phys. Rev. B* **17**, 726 (1978).
- <sup>19</sup>S.-C. Hong, G. P. Kothiyal, N. Debbar, P. Bhattacharya, and J. Singh, *Phys. Rev. B* **37**, 878 (1988).
- <sup>20</sup>C. Mailhot, and D. L. Smith, *Solid State Mater. Sci.* **16**, 131 (1990).
- <sup>21</sup>B. Gil, P. Lefebvre, P. Boring, K. J. Moore, G. Duggan, and K. Woodbridge, *Phys. Rev. B* **44**, 1942 (1991).
- <sup>22</sup>J. Lee and M. O. Vessel, *Can. J. Phys.* **66**, 1088 (1988).
- <sup>23</sup>J. Lee and M. O. Vessel, *Phys. Rev. B* **37**, 8855 (1988); **37**, 8861 (1988).
- <sup>24</sup>S. L. Chuang, *Phys. Rev. B* **43**, 9649 (1991).
- <sup>25</sup>G. E. Bauer and T. Ando, *Phys. Rev. B* **38**, 6015 (1988).
- <sup>26</sup>L. C. Andreani and A. Pasquarello, *Phys. Rev. B* **42**, 8928 (1990).
- <sup>27</sup>D. A. Broido and S.-R. E. Yang, *Phys. Rev. B* **42**, 11 051 (1990).
- <sup>28</sup>D. Ahn and S. L. Chuang, *IEEE J. Quant. Electron.* **QE-24**, 2400 (1988).
- <sup>29</sup>T. C. Chong and C. G. Fonstad, *IEEE J. Quant. Electron.* **QE-25**, 171 (1989).
- <sup>30</sup>J. M. Luttinger and W. Kohn, *Phys. Rev.* **97**, 869 (1955).
- <sup>31</sup>J. M. Luttinger, *Phys. Rev.* **102**, 1030 (1956).
- <sup>32</sup>D. A. Broido and L. J. Sham, *Phys. Rev. B* **31**, 888 (1985).
- <sup>33</sup>A. T. Twardowski and C. Herman, *Phys. Rev. B* **35**, 8144 (1987).
- <sup>34</sup>*Numerical Data and Functional Relationships in Science and Technology*, edited by K.-H. Hellwege, Landolt-Börnstein, New Series, Group III, Vol. 17a (Springer, Berlin, 1982); Groups III-V, Vol. 22a (Springer, Berlin, 1986).
- <sup>35</sup>C. D. Lee and S. R. Forrest, *Appl. Phys. Lett.* **57**, 469 (1990).
- <sup>36</sup>C. Y.-P. Chao and S. L. Chuang, *Phys. Rev. B* **43**, 7027 (1991).
- <sup>37</sup>B. K. Ridley, *J. Appl. Phys.* **68**, 4667 (1990).
- <sup>38</sup>I. Suemune, *Phys. Rev. B* **43**, 14 099 (1991).
- <sup>39</sup>B. Zhu and K. Huang, *Phys. Rev. B* **36**, 8102 (1987); B. Zhu, *ibid.* **37**, 4689 (1987).